Autonomous Demand Smoothing for Efficiency Improvements on Military Forward Operating Bases

Spencer C. Shabshab, Peter A. Lindahl, Steven B. Leeb, and J. Kendall Nowocin

***Abstract*—This paper presents autonomous control algorithms for electrical loads like HVAC (Heating, Ventilation, and Air Conditioning) systems. These algorithms permit a load to become "aware" of the operation of neighboring loads using nonintrusive measurements of the utility voltage. Analogous to the way a good driver is aware of neighboring cars while driving, loads can use this information to become "self-driving." For HVAC systems, this permits maintaining occupant comfort while simultaneously reducing bulk peak electrical demand. Electric energy consumption for each load occurs on a schedule, interleaved with the operation of neighboring units. The algorithms are demonstrated here using simulation models developed from nonintrusive load monitoring (NILM) data collected from the microgrid of a US Army forward operating base (FOB). The general approach, however, can be applied in many other venues, e.g., to minimize peak load on distribution transformers in a section of the conventional utility.**

***Index Terms*—Microgrids, smart grids, demand-side management, centralized control, heating systems, temperature control, nonintrusive monitoring.**

I. Introduction

LARGE power consuming loads are targets for energy-saving demand response schemes [1]. Loads amenable to demand response scheduling include deferrable loads, thermal loads that can be delayed subject to acceptable temperature bounds [2], and curtailable loads, which can be completely switched off until needed. Associated demand response schemes often require centralized optimization based on aggregated inputs and knowledge of load type to produce distributed tasking orders or load scheduling across energy consumers [3], [4].

Grids or sections of power grids may be resource constrained for different reasons. True microgrids on land, such as the US Army FOBs, or elsewhere, e.g., on ships or aircraft, are constrained by generation resources. These constraints include absolute power limits and also a desire for efficient operation. Sections of other grids may be effectively constrained by distribution components like transformers. This paper has demonstrated algorithms for optimizing grid loading without exceeding grid capability. It is essential to consider the performance of the algorithms developed here in comparison to other approaches. Substantial efforts have been reported to optimize grid loading.

In microgrids characterized by fast changing load demands, generators may not dispatch quickly enough to effectively match generation to demand, and the load profile needs reshaping to improve overall efficiencies. Incorporating *extrinsic* energy storage devices, e.g., batteries, into diesel generator or hybrid powered microgrids can accomplish this but at the expense of additional capital costs [5], [6]. Load management schemes can leverage the "free" *intrinsic* energy storage capacity associated with loads, e.g., those of the water in hot water heaters [7], [8] and the structures served by Environmental Control Units (ECUs) [2], [9]. Such schemes have been broadly investigated for reducing peak demands [2], [7], [10] on the utility scale.

Reference [11] designed a power electronic-based energy management system for an FOB to efficiently dispatch multiple generators, batteries, and non-critical loads. This manager was later expanded to accommodate photovoltaics and optimized to minimize energy use [12]. In this approach however, load management was only used to curtail non-critical loads rather than time-shift individual loads. More recently, Reference [13] developed a simulation model of a 45-person Marine Corps FOB containing several shelters, multiple generators of varying capacity, and a battery-based energy storage system. He then used a mixed-integer linear programming (MILP) approach to schedule ECU run-times in an effort to optimize generator dispatch. Reference [14] furthered this research by analyzing the efficiency improvements of such an optimization scheme with the addition of renewables and the presence of uncertainty in demand scheduling.

Each of these approaches requires additional control or energy storage hardware or both.

Analogous to the way a good driver is aware of neighboring cars, there exists an opportunity for creating "self-driving" loads that are aware of the operation of other local loads. Particularly on a microgrid, important energy consumers can detect the operation of neighboring loads without special information or control wiring [15]. This paper proposes algorithms for "autonomous demand response" schemes that permit loads to naturally optimize the overall energy consumption of the aggregate group. These algorithms have been developed and validated with models derived from a microgrid serving a US Army forward

Manuscript received September 7, 2019; revised November 3, 2019; accepted January 4, 2020. Date of publication January 7, 2020; date of current version September 23, 2020. This work was supported by The Grainger Foundation and Exelon under an MITei-Exelon research agreement. Paper no. TPWRD-01016-2019. *(Corresponding author: Steven Leeb.)*

S. C. Shabshab is with the MIT, Cambridge, MA 02139 USA (e-mail: doubleshab@gmail.com).

P. A. Lindahl is with the Naval Nuclear Power Training Command, US Navy, Charleston, SC 29404 USA (e-mail: plindahl@exponent.com).

S. B. Leeb is with the RLE, MIT, Cambridge, MA 02139 USA (e-mail: sbleeb@mit.edu).

J. K. Nowocin is with the Exponent Inc, Natick, MA 01760 USA (e-mail: kendall.nowocin@gmail.com).

Color versions of one or more of the figures in this article are available online at http://ieeexplore.ieee.org.

Digital Object Identifier 10.1109/TPWRD.2020.2964702

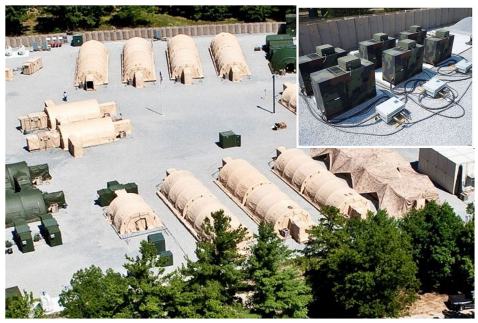

Fig. 1. Aerial photograph of the BCIL; the inset photo in the upper right shows interconnected generators powering the BCIL microgrid.

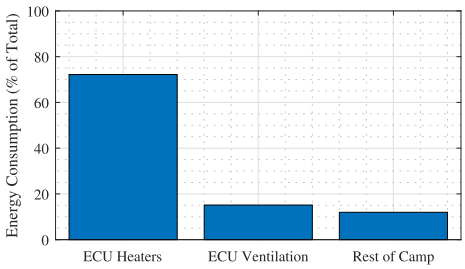

Fig. 2. Load breakdown at BCIL by power consumption.

operating base (FOB). However, the techniques proposed here could be applied on subsections of a conventional utility or other power system.

II. Energy Savings Opportunity on an Army FOB

Fig. 1 shows an aerial view of the Base Camp Integration Laboratory (BCIL) FOB, which the US Army uses to test new technologies for potential deployment to FOBs around the world. The BCIL contains generation resources, service loads, and habitable structures. Each "Quonset-hut" style tent complex (Fig. 1) is comprised of two connected tents, with each tent's temperature maintained by an individual ECU. The inset picture in the upper right corner shows a bank of interconnected diesel generators that serve the FOB microgrid.

Nonintrusive load monitoring (NILM) [16] devices gathered data at the BCIL FOB over a period of several years to observe and characterize the electrical demand [17], [18]. In cold weather, the FOB's energy demand is dominated by the camp's ECUs. As shown in Fig. 2, during heating operation, the ECU heaters account for over 70% of the total base load.

Fig. 3 illustrates the opportunity to reduce energy expenditures at the base through autonomous load coordination. Fig. 3(a) shows the power draw at the BCIL over a two hour window while the base was occupied by 90 soldiers [15]. The blue area shows the total non-ECU heater load, while the red area shows the cumulative ECU heater load. During this time period, the non-ECU heater load was stable but the cumulative ECU heater load varied significantly as the number of simultaneously operating ECUs varied. The average load during this period was 44 kW but the peak load was over 70 kW.

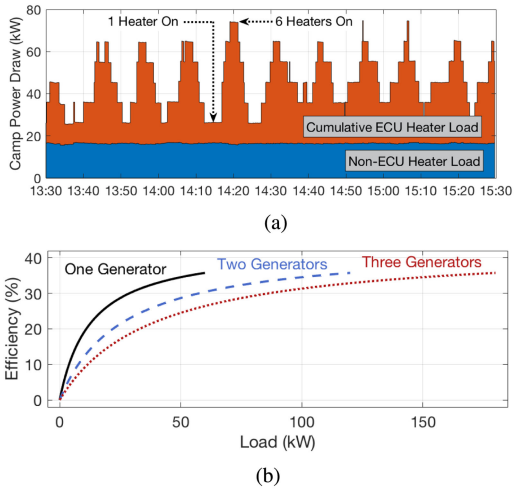

Fig. 3. Coincidental ECU operations cause large peak loads and inefficient generator operation [15]. The top plot depicts how simultaneous ECU heater operations far exceed the average ECU demand over the time window. The plot of (b) depicts efficiency curves for paralleled 60 kW diesel generators. To meet the needs of the aggregate load with frequent peaks requires excess generators leading to inefficient fuel use. (a) Camp Load. (b) Generator Efficiency.

These peaks are caused by the conventional thermostatic control employed by the ECUs to regulate the tent temperatures. Each ECU is controlled with a hysteretic or thermostatic control with high and low setpoints. Similar to the behavior in most residential or commercial venues, the ECU control systems receive no coordination. They simply respond to temperature conditions in the structure that they serve. The "random" timing of each ECU activation leads to a sliding phase of operation with respect to other ECUs on the base. Periodically, many ECUs (as many as six of the camp's eight ECUs online during this time window) will be "on" at the same time, putting a maximum demand on the microgrid. This operating profile is unfortunate as it requires two generators to support the grid instead of just one and results in less efficient fuel use.

Except under the most extreme environmental conditions, no HVAC or ECU system needs to operate continuously without pause. The operation of the ECUs could instead be interleaved to minimize peak demand while maintaining occupant comfort. In Fig. 3, no more than three ECUs need to operate simultaneously to maintain occupant comfort. In this case, the aggregate load could be met by a single generator resulting in an efficiency improvement of 18% [15].

This new control scenario is called *the potato game*. A utility or other operator could call out a maximum number of "potatoes," i.e., active ECUs, that could be tolerated during a given operating window of time for the utility. "Well-behaved" ECUs could be made "aware" of the operation of other ECUs and could wait for their turn to "grab a potato" when one becomes available, i.e., a different ECU turns off. The ECU that had been waiting could then operate to provide needed HVAC service. If all ECUs are well behaved, the peak power demand is minimized without requiring specially coordinated control across the ECUs. On an Army FOB, this autonomous coordination could mean operating one generator efficiently rather than wasting fuel with

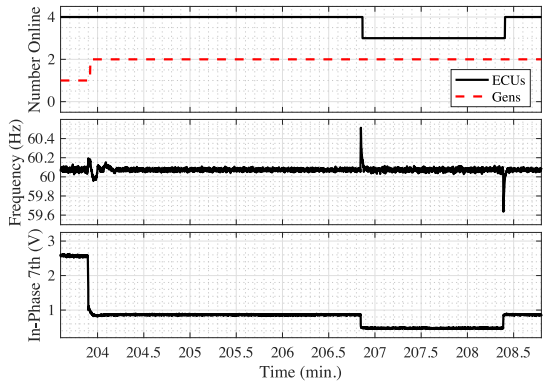

Fig. 4. Demonstration of the event identifier successfully recognizing events in actual data from BCIL [15].

two inefficiently loaded generators operating to meet occasional peak demand. On the conventional utility, this type of coordination across residences, for example, could mean the difference between operating or overloading a distribution transformer.

III. Opportunity for Grid Event Detection

A foundational tool for creating autonomous loads capable of playing the "potato game" is some mechanism by which each load in the game can deduce information about the states of the other loads on the grid. This information could be shared via a dedicated communication network, but an alternative and intriguing possibility is to create "awareness" through the observation of the utility voltage waveform itself, with no other special information exchanged. Telltale changes in the utility voltage waveform can be identified in real-time to identify the operation of neighboring loads. In this case, the utility serves as both the source of power and also as a signaling network. This approach works particularly well on microgrids or sections of the conventional utility where the voltage regulation is not perfectly "stiff." Demonstration of the application of these nonintrusive identification techniques, presented in [15], will be employed later in this paper to make loads on the microgrid aware of the operation of neighboring loads in real-time.

Reference [15] presents an event identification technique that permits a load to nonintrusively recognize the operation of neighboring loads by identifying power quality changes in the voltage shared by the loads. This event detection algorithm requires no special control wiring or networking. Fig. 4 depicts the operation of the event identifier from [15]. The top plot depicts the identifier output as it tracks the number of ECU heater loads online and the number of diesel generators dispatched. The middle plot shows the frequency of the microgrid utility at BCIL. There are distinct deviations as the generators and ECUs activate and deactivate. These frequency deviations occur because the BCIL generators do not have over-sized spinning energy reserves in comparison to the load requirements. The bottom plot provides the measured in-phase 7th harmonic content in the BCIL's microgrid voltage. This voltage distortion is due to the power electronics of the ECU fan drives and the space harmonics in the rotating machinery of the generators. Its level changes as loads and generators come on and off-line. Together, the frequency variations and changes in 7th harmonic content provide "fingerprint signatures" useful for distinguishing the turn-on/off of ECUs and the addition or removal of a generator from the generator pool. In Fig. 4, the small frequency fluctuation and large 7th harmonic step change at approximately 204 mins corresponds to a generator turn-off event. Later, the positive frequency spike / small negative 7th harmonic step and negative frequency spike / small positive 7th harmonic step correspond to ECU heater turn-off and turn-on events, respectively.

Generally, the ability of a controller to recognize these signatures as identifiable events can be approached as a machine-learning problem, similar to those of current-based event identification, e.g., [19], [20]. However, given limited labelled event data due to restrictions in BCIL access, a cross-correlation-based approach was developed for recognition of frequency and 7th harmonics transients using representative event transients, i.e., "exemplars" [15].

Once a candidate event is identified, segments of the measured frequency and 7th harmonic data streams containing the event are compared against frequency and 7th harmonic exemplars for each of the following events, an ECU turn-on, an ECU turn-off, a generator turn-on, and a generator turn-off. This comparison is quantified with a matching score,

$$S = \frac{\sum_{n=0}^{N-1} \left(x[n] - y[n + l_o]\right)^2}{\sum_{n=0}^{N-1} x\,[n]^2}. \tag{1}$$

Here, $x[n]$ is an exemplar waveform (either freq. or 7th harm.) of sample-length N, and $y[n + l_o]$ is an equivalent-length section of the corresponding data stream sample-shifted by,

$$l_o = \underset{l}{\operatorname{argmax}} \sum x[m]y[m + l]. \tag{2}$$

Combined, (2) ensures the two waveforms are time-aligned by identifying the sample-delay, l_o which maximizes the correlation between the two signals, and (1) scores the extent to which the two waveforms match. A perfect score, $S = 0$, occurs when the two signals are identical. Maximum scores below which a measured transient is deemed to match the exemplar and above which it is not were defined empirically. For the BCIL, a maximum matching threshold of $S_{\max} = 0.2$ for all 7th harmonic transients corresponded to any event type and all frequency transients corresponding to all event types except generator turn-on events. For these, the maximum score threshold was set to $S_o = 0.45$ as these frequency transients are less distinct.

Given the ability to recognize the operational events of neighboring loads, a new kind of controller can be created to accompany each load. This controller can automatically respond intelligently to the behavior of other loads in order to minimize utility demand. The algorithms presented here work nonintrusively, but can also be used with loads that communicate by dedicated networks or any other convenient means.

IV. Autonomous ECU Control Framework

Fig. 5 provides the state diagram of an ECU heater. Under traditional thermostatic control, the ECU heater only changes states

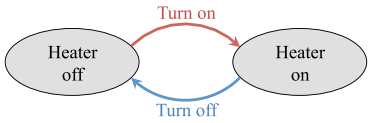

Fig. 5. ECU heater state diagram.

TABLE I
HEATER INTERRUPT ROUTINES IN ORDER OF PRECEDENCE FOR EACH STATE

State	Interrupt Service Routine	Trigger
Heater off	1. Transient identification	Transient event detected
	2. Under-temperature	$T_t < T_l$
Heater on	1. Transient identification	Transient event detected
	2. Over-temperature / Overlength	$T_t > T_h$ OR $t_{on} > t_{on,max}$

in response to the temperature of the tent. Specifically, when off, the heater will turn on only when the temperature inside the tent, T_t, decreases below a lower temperature threshold, T_l, and when on, the heater will only turn off when the temperature rises above an upper threshold, T_h. While simple and robust, this type of control creates the large aggregate demand peaks depicted in Fig. 3, which can lead to inefficiencies and excess strain on grid distribution equipment.

A self-distributing, autonomous ECU can maintain the temperature responsiveness of the traditional thermostatic control but also improve the collective behavior of the units by limiting the number of simultaneously operating ECUs. Interrupt service routines (ISRs) were used to create autonomous ECU control framework that takes into account both temperature information and knowledge of the operational states of the grid's generators and other ECUs. Under this autonomous control regime, each ECU controller constantly monitors its tent's temperature and its local voltage, processing the latter for frequency and 7th harmonic data streams. Both the temperature and voltage quality information can "trigger" interrupt service routines, which update the ECU's knowledge of the grid state and/or cause the ECU heater to change states.

Table I lists these routines for each ECU heater state, in order of "precedence," along with the trigger event that causes their operation. In both states, the transient identification routine takes precedent over the temperature-based routines. That is, if a transient event is detected (triggered) while the ECU controller is executing a temperature-based routine, the controller will abort and execute the transient identification routine before reinitiating the temperature-based routine.

A. Temperature-Based Routines

Considering first the under-temperature interrupt service routine, Fig. 6 depicts its operational flowchart for the under-temperature routine, which triggers when $T_t < T_l$. However, unlike traditional thermostatic control, this condition alone only initiates the routine rather than ensures the heater turns on. Under the autonomous control scheme, the ECU controller considers the operation mode of the ECU and if the tent temperature has dropped below a second, lower threshold, T_{l2}. The two operating modes of the ECU are startup, i.e., when the ECU is first turned

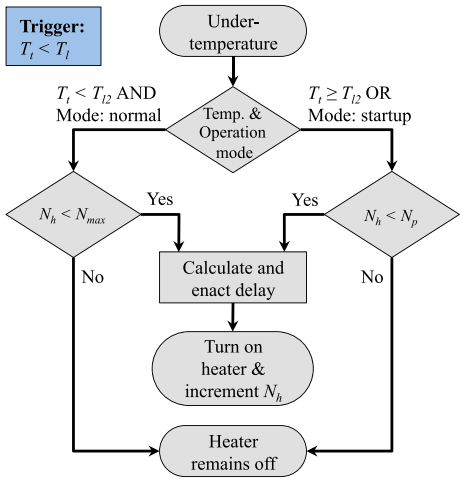

Fig. 6. Under temperature interrupt routine.

on to regulate tent temperature (in contrast to the operation state of its heating element), and normal operation, which the ECU switches to after first eclipsing the lower temperature threshold, T_{l2}.

During startup, or if the tent temperature is above its lower temperature threshold, the ECU heater can turn on (following a delay) if the number of other heaters in their on state, N_h, is less than the total number of available "potatoes," N_p. If the ECU is operating in normal mode and the temperature further drops below T_{l2}, the heater can turn on if doing so will not cause the total number of on heaters to exceed a maximum number, $N_{\max}$. This lower temperature threshold allows the ECU to autonomously "shed load," prioritizing limiting the aggregate ECU power demand, until the tent temperature drops to a minimum comfort level. At that point, the ECU prioritizes thermal comfort and will turn on the heater so long as doing does not risk exceeding the total available generation capacity ($N_{\max}$ is set based on the number of available generators and their total capacity).

Importantly, prior to turning its heater on, the ECU controller enacts a delay, with the length of the delay dependent on the tent's temperature error,

$$T_e = T_t - T_s, \tag{3}$$

where T_s is the target temperature setpoint for the tent. This time-dependent delay is calculated as,

$$t_d = \begin{cases} t_o + mT_e, & \text{if } T_e < \frac{t_{\min} - t_o}{m} \\ t_{\min}, & \text{otherwise} \end{cases}. \tag{4}$$

Here, t_o, m, and $t_{\min}$ are positive values representing the offset and slope of the delay's relationship with temperature error in its linear region, and an optionally set minimum temperature delay, respectively.

The over-temperature / overlength interrupt service routine (Fig. 7) enacts control similar to thermostatic control in response to the tent temperature eclipsing a high temperature threshold

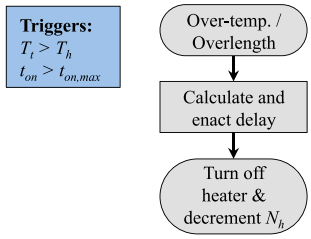

Fig. 7. Over temperature / overlength interrupt routine.

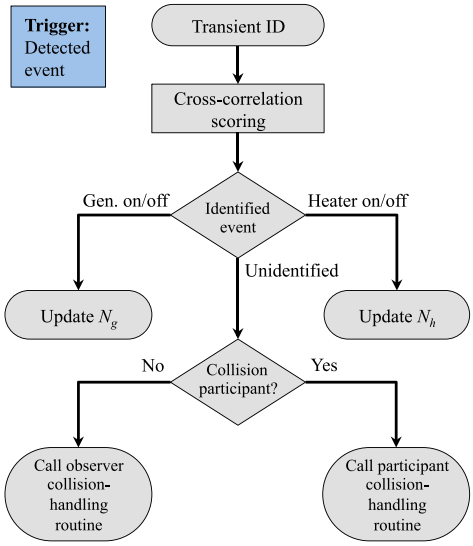

Fig. 8. Transient identification routine.

level, though the routine also imparts an error-dependent time-delay,

$$t_d = \begin{cases} t_o - mT_e, & \text{if } T_e < \frac{t_{\min} - t_o}{m} \\ t_{\min}, & \text{otherwise} \end{cases}. \tag{5}$$

The delay timer in both of these temperature-based routines allows the ECU most in need to take action first.

One final note regarding the over-temperature / overlength interrupt service routine is that it can also be triggered if the time that an ECU's heater is on, t_{on}, exceeds a maximum threshold, $t_{on,\max}$. This rule enforces resource sharing among the autonomous ECUs. Similar to the delay-times, the maximum on-time can be made dependent on temperature error to promote increased resource sharing allocation to the tents that most require heat.

B. Transient Identification Routine

The transient identification routine depicted in Fig. 8 is triggered when an event is detected in either or both of the frequency or 7th harmonic data streams. If an event is identified as a generator or ECU on/off event according to its cross-correlation scores, the routine updates the ECU controller's knowledge of the microgrid state accordingly. When the ECU does not recognize the event, its either because the event was caused by one or more unmonitored loads, or because an ECU or generator changed states at nearly the same as did another ECU, generator or unmonitored load. This latter case is an "event collision". To rectify the ambiguity, each ECU calls one of two collision-handling routines (Fig. 9), depending on if it participated in the collision (i.e. it changed states at the time of the unidentified event) or just observed it.

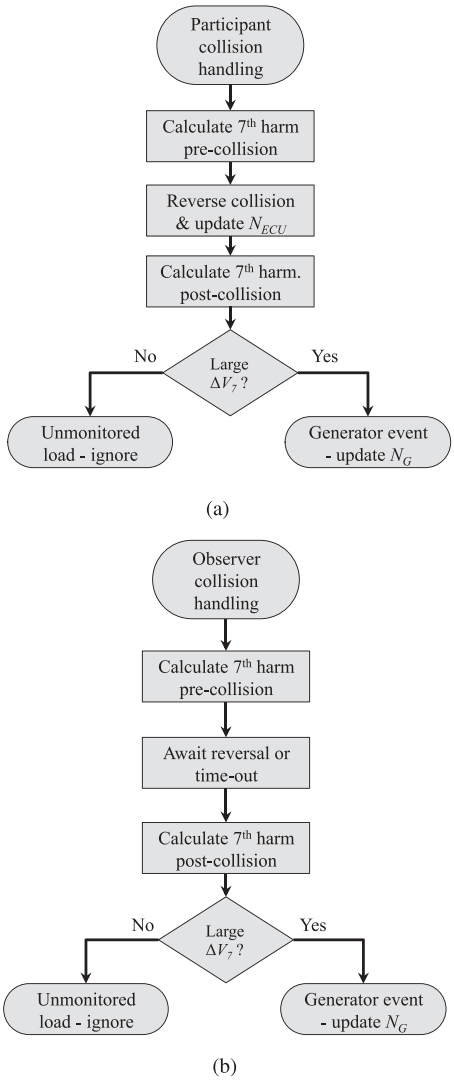

Fig. 9. Collision-handling routines call for any autonomous ECU collision participants to revert back to their pre-collision states and for the observers to monitor for the reversal. From the difference between pre-collision and post-collision 7th harmonic voltage measurements, the ECUs can also detect if a generator event was involved in the collision. (a) Participant Routine. (b) Observer Routine.

The function of these collision-handling routines are to reverse all controllable actions which contributed to the collision, and to determine whether any uncontrolled events of interest (generator turn-on or turn-off events, in this case) also contributed. To begin, both collision participants and observers log the average value of their 7th harmonic streams for the one second preceding the unidentified transient. Following this, the collision participants reverse their actions (e.g. heaters that turned on, turn back off) and update their N_h counts to comply

with the reversal. Importantly, this action also restores the accuracy of the other autonomous ECUs as they will not have recognized the collision event. Once this reversal concludes (assessed by observers either by witnessing the reversal or after a set length of time), each ECU measures the 7th harmonic stream again for comparison with pre-collision levels. Because any ECUs involved have reversed their actions, there is no difference in the number of ECU heaters operating during these two measurements, and only uncontrolled loads or generator events will have caused differences in the 7th harmonic measurements. The effect of generator events on the 7th harmonic is significant larger than those of uncontrolled events, and thus the controller determines generator event participation based on the size of the difference between the pre-transient and post-transient 7th harmonic measurements.

V. Simulation Environment for Control Evaluation

A simulation environment capturing the electrical interactions between the ECUs and FOB generators was developed from our nonintrusive monitor data and used to validate the proposed control algorithms. The simulation system, developed in MATLAB, is made up of modular dynamic electrical generator models and thermal energy transfer models of the BCIL tent structures. Collectively, these models reproduce the power quality signatures associated with the generator and ECU interactions. The simulation system also allows the incorporation of synthetic or measured weather data, e.g., solar irradiance and outdoor temperature measurements collected at the BCIL weather station. This modularity permits quick testing of proposed algorithms in many different emulated environments, thus affording algorithm testing without having to wait months or years for random chance to provide particular operating scenarios for weather, tent condition, generator configuration, and load mix.

A. Generator Model

The BCIL generator bank consists of 6 paralleled units, each a 60 kW synchronous diesel generator, directly connected to the microgrid through interruption contactors. Several of these generators are redundant and installed to allow for maintenance and equipment rotation. The generators spin-up and down according to their automatic dispatch rules, which work to keep the load below 80% of the real-time generation capacity and above 60% of the future generation capacity if one generator were to go off-line. Time delays ensure that an additional generator comes on-line after 10 seconds of loading in excess of the 80% metric, and a generator spins-down after five minutes of load below the 60% metric. This control attempts to balance efficiency (better at high load) while also protecting the generators from overload in the event of sudden demand increases.

A modified fourth-order synchronous machine model adequately reproduces the frequency deviations of the BCIL generators. Full descriptions for the model's inputs, state variables, and parameters, along with the values used for simulating the generators at BCIL are available in [15]. Changes in the number of on-line generators are accommodated in the model, which scales the armature and inertia associated with the simulated

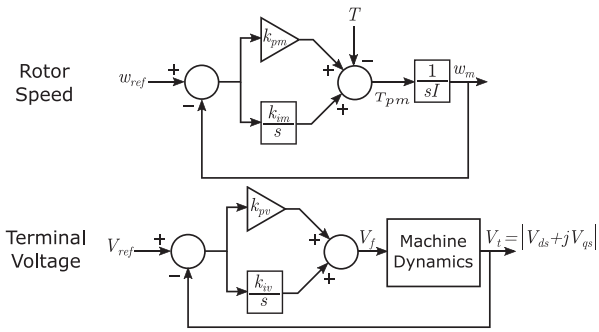

Fig. 10. PI feedback control of synchronous terminal voltage and rotor speed.

generator model to account for the paralleling or disconnection of a generator. To incorporate the observed transient dynamics, the mechanical torque T_{pm} and the generator field excitation V_f are each modeled to be controlled by feedback of the rotor speed ω_m and the terminal voltage (V_t), respectively (Fig. 10). The control loops and feedback gains shown in Fig. 10 are a function of the generator design for the microgrid. These controls are not assumed to be adjustable. That is, the proposed autonomous demand response algorithm is designed to operate with the generators as they are configured for the grid, without additional changes.

The load seen by the generator model is determined by the state of all connected loads. These include the ECUs as well as the other camp loads, the vast majority of which are smaller than the ECUs and don't create transients easily confused with ECU transients. The primary exception to this rule is the latrine pump, which draws a large in-rush current when turned on resulting in transients of similar size and shape to ECU on transients. Pump transients were included in the simulation to challenge the transient event identifier.

Changes in the total load alter the simulated power draw from the generators. In accordance with the generator dispatch rules, this can trigger the number of on-line generators, N, to change as well, resulting in the scaling of the armature and inertia associated with the effective generator model.

The outputs of the simulator include a time-series of microgrid frequency and also 7th harmonic content. Transients in these two time series serve as input to the transient event detector, which identifies events that occur as it would at the actual BCIL.

To simulate the 7th harmonic voltage stream, a 4th order polynomial was fit to the measured data collected at the BCIL. This stream was observed to be primarily a function of the number of online generators, N, and of the total power demand normalized to generation capacity, ρ_l [15]. This relationship is well modeled by,

$$V_7 = c_{p4}\rho_l^4 + c_{p3}\rho_l^3 + c_{p2}\rho_l^2 + c_{p1}\rho_l + c_N N + c_0 + e \quad (6)$$

where e is a Gaussian-distributed random variable simulating measurement noise. Table II provides parameter values.

B. Tent Model

The simulator also models the dynamic thermal performance of the tent structures (each tent is comprised of two tents

TABLE II
SEVENTH HARMONIC CURRENT MODEL PARAMETERIS

Coefficient	Value
c_{p4}	9.8×10^{-8}
c_{p3}	-2.3×10^{-5}
c_{p2}	0.0017
c_{p1}	0.0124
c_N	-0.66
c_0	0.54
Measurement noise, e	
Mean	0
Std.	0.05 V

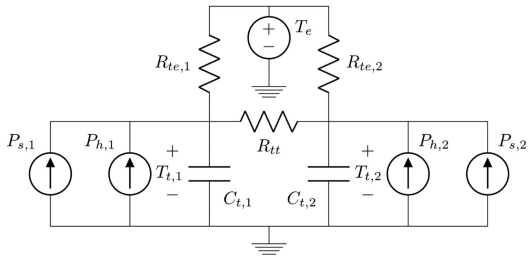

Fig. 11. Tent complex model. Subscripts '1' refer to tent Section I, subscripts '2' refer to tent Section II.

connected back-to-back as shown in Fig. 1). Here, the thermal capacitances, $C_{t,i}$, represent the two tents ($i = 1$ and $i = 2$), with internal temperatures, $T_{t,i}$. Each tent's thermal capacitance depends on its contents, which may include tables, desks, bunks, and other equipment. The tents interact with the outside environment, represented here as a thermal reservoir, T_e, via the thermal impedances, $R_{te,i}$. The tents also absorb heat sourced from the sun ($P_{s,i}$) and exchange heat with each other through convective heat flow (R_{tt}). Each tent's ECU provides heat ($P_{h,i}$) to its tent.

These ECU heaters are two-stage heat sources normally under thermostatic bang-bang control with rated output power, $P_{h,rated} = 9$ kW when on and 0 kW when off. Due to heated air needing to propagate from the ECU output through a duct and into the tent section before heating occurs, the rate of heat supplied from the ECU to the tent follows the first order differential equation,

$$\dot{P}_{h,i} = \frac{1}{\tau_{h,i}}(P_{h,rated} - P_{h,i}), \tag{7}$$

where, $\tau_{h,i}$ is a time constant related to the time required to move this heated air.

The rate of solar heat absorption in each tent is proportional to the local solar irradiance, P_{sol} through the scaling constant, $k_{s,i}$, which accounts for the location and orientation of each tent section relative to the sun, i.e.,

$$P_{s,i} = k_{s,i} P_{sol}. \tag{8}$$

Using the **greyest()** command in MATLAB along with data collected at the BCIL, including environmental temperature, solar irradiance, heater states, and tent temperatures, parameters were fit to the tent complex models of Fig. 11 and (7) and (8) to the thermal performance of four tent complexes. Table III shows the extents of the parameter value fits, while Fig. 12 compares

TABLE III
TENT COMPLEX MODEL PARAMETERS

	$C_{t,i}$ (kJ/K)	$R_{te,i}$ (K/kW)	R_{tt} (K/kW)	$k_{s,i}$ (W/m^2)	$\tau_{h,i}$ (s)
Max	444	2.27	4.0	22.1	91
Min	332	1.76	2.3	9.8	43.5

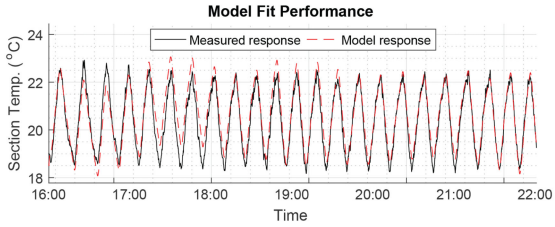

Fig. 12. Model fit performance for a tent.

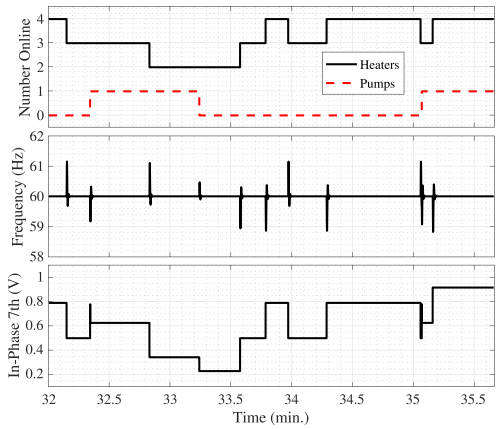

Fig. 13. Simulated grid frequency (middle) and in-phase 7th harmonic (bottom) in response to the the microgrid events of the top plot. This top plot is the output of the voltage transient identification algorithm, which uses the frequency and 7th harmonic streams for identifying ECU, generator, and latrine pump operations.

the resulting temperature estimates to measured data for one of the tents over a six hour window.

C. Simulator Performance

With models for the generator bank and tent dynamics, the simulator is able to produce time-series outputs of the microgrid electrical frequency and 7th harmonic content in response to changes in the camp's load. Fig. 13 shows a representative three minute and a half minute example of this. During this time segment only one generator is on-line. The top plot shows the operational status of the camp's ECU heaters and latrine pumps as detected by the transient identifier, while the middle and bottom plots show the frequency and 7th harmonic stream transients indicating these load changes, respectively. These responses are qualitatively identical to the field observations at BCIL, e.g., those shown in Fig. 4.

VI. DEMAND SMOOTHING

To validate the autonomous ECU control concept, a camp of eight tents serviced be eight ECUs was simulated for six

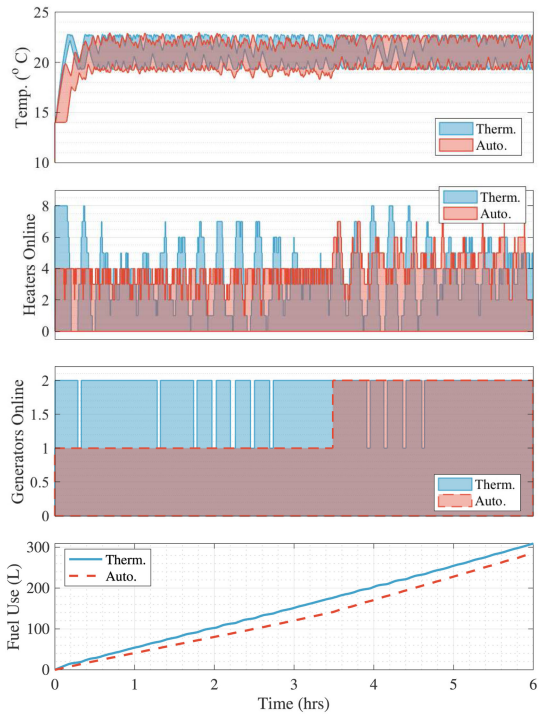

Fig. 14. Simulation of eight tent camp under thermostatic (blue) and autonomous (red) control.

hours of operation under both traditional thermostatic control and the autonomous ECU control concept (Fig. 14). During this time period, the environmental temperature starts at 14 °C and then ramps down to 12 °C starting at the two hour mark and ending at the four hour mark after which the temperature remains at 12 °C. Over the first two hours, with the environmental temperature 14 °C, both the traditional thermostatic controllers and the autonomous ECU controllers keep tent temperatures between 19 and 23 °C. These are the set T_l and T_h values, respectively. Contrary to the traditional thermostatic control however, the autonomous ECU controllers distribute the ECU heater operations such that no more than four ECUs operate at any time (N_p). This results in a lower rate of fuel use as only one generator needs to be online.

Between the two and four hour marks, the tent temperatures in the autonomous control simulation drift slightly below 19 °C as the ECU controllers are unable to simultaneously restrict the number of operating ECUs and maintain tent temperatures above T_l. Around the 3.5 hour mark, the tent temperatures reach T_{l2} resulting in thermostatic override and more than $N_p = 4$ number of heaters simultaneously operating. This causes the 2nd generator to turn on and N_p to correspondingly increase. The easing of the restriction on the number of simultaneously operating tents allows the tent temperatures to recover. During this time period, the autonomously controlled tents continue to demand less fuel use of the generators compared to the traditional thermostatically controlled tents, at the expense of a slight compromise in tent temperatures. This exercise illustrates the stability of the autonomous control, and the flexible trade-off provided to the facility manager. For any given environment conditions, a particular band of preferred tent temperature between T_l and T_h will require a certain duration of ECU operation in each tent. Adequate selection of N_p results in the most efficient use of generating resources while maintaining temperature comfort. This situation occurs in the first two hours of the demonstation. If N_p is intentionally set to a tighter number than needed by the environmental conditions, than the algorithm favors fuel conservation at the slight expense of tent temperature control as shown between hours 2 and 3.5 in the experiment. Finally, if N_p is increased, tighter control can be maintained on tent temperature in the face of extreme environmental conditions, with the associated requirement for enhanced generating resources as shown in the final two and a half hours of the experiment. The algorithm provides stable operation for any facilities management preference.

Finally, during the four and six hour marks, the autonomously controlled ECUs operate similarly to the thermostatically controlled ones. Over the course of this six hour segment, the simulated camp with ECUs under autonomous control use 20 L less fuel (approx. 7% savings) than the camp with ECUs under thermostatic control. Additional simulation examples for other contingency conditions on the grid and for other load signatures, including the presence of confounding loads like a resistor bank on the grid, can be found in [15] and [21].

VII. Conclusion

This paper presents new load management algorithms that can be retrofit, in many cases as primarily software changes, in the controllers of existing loads. Hardware changes for the approach demonstrated here can be as simple as a single voltage sensor, or no hardware change at all in loads that include input voltage monitoring (e.g., power electronic controlled systems). At the Army microgrid, the heating loads operate under "bang-bang" control, and our algorithm requires no further control complexity in the basic operation of the ECU to add new autonomous demand response features. Of course, more sophisticated ECU's with variable controls or variable speed drives could offer additional degrees of freedom for maintaining temperature and minimizing grid loading. The algorithms presented here serve as the basis for improving energy efficiency and reducing fuel or energy demand. Installation effort is minimal, requiring no networked communication. The approaches presented here create "self-driving" loads that are intrinsically aware of the operation of other loads on the utility.

Acknowledgment

The authors grateful acknowledge the valuable support and advice of W. Singleton and the operations team that supports the US Army Base Camp Integration Laboratory at Ft. Devens.

References

[1] S. Althaher, P. Mancarella, and J. Mutale, "Automated demand response from home energy management system under dynamic pricing and power and comfort constraints," *IEEE Trans. Smart Grid*, vol. 6, no. 4, pp. 1874–1883, Jul. 2015.

[2] N. Lu, "An evaluation of the hvac load potential for providing load balancing service," *IEEE Trans. Smart Grid*, vol. 3, no. 3, pp. 1263–1270, Sep. 2012.

[3] C. Eksin, H. Delic, and A. Ribeiro, "Demand response management in smart grids with heterogeneous consumer preferences," *IEEE Trans. Smart Grid*, vol. 6, no. 6, pp. 3082–3094, Nov. 2015.

[4] Y. Zhang and N. Lu, "Parameter selection for a centralized thermostatically controlled appliances load controller used for intra-hour load balancing," *IEEE Trans. Smart Grid*, vol. 4, no. 4, pp. 2100–2108, Dec. 2013.
[5] P. Arun, R. Banerjee, and S. Bandyopadhyay, "Optimum sizing of battery-integrated diesel generator for remote electrification through design-space approach," *Energy*, vol. 33, pp. 1155–1168, 2008.
[6] E. Hittinger, T. Wiley, J. Kluza, and J. Whitacre, "Evaluating the value of batteries in microgrid electricity systems using an improved energy systems model," *Energy Conv. Manage.*, vol. 89, pp. 458–472, 2015.
[7] S. Pourmousavi, S. Patrick, and M. Nehrir, "Real-time demand response through aggregate electric water heaters for load shifting and balancing wind generation," *IEEE Trans. Smart Grid.*, vol. 5, no. 2, pp. 769–778, Mar. 2014.
[8] Z. Xu, R. Diao, S. Lu, J. Lian, and Y. Zhang, "Modeling of electric water heaters for demand response: A baseline PDE model," *IEEE Trans. Smart Grid*, vol. 5, no. 5, pp. 2203–2210, Sep. 2014.
[9] M. Avci, M. Erkoc, A. Rahmani, and S. Asfour, "Model predictive hvac load control in buildings using real-time electricity pricing," *Energy Build.*, vol. 60, pp. 199–209, 2013.
[10] A. Safdarian, M. Fotuhi-Firuzabad, and M. Lehtonen, "Optimal residential load management in smart grids: A decentralized framework," *IEEE Trans. Smart Grid*, vol. 7, no. 4, pp. 1836–1845, Jul. 2016.
[11] R. Kelly, G. Oriti, and A. Julian, "Reducing fuel consumption at a remote military base: Introducing an energy management system," *IEEE Electrific. Mag.*, vol. 1, no. 2, pp. 30–37, Dec. 2013.
[12] N. Anglani, G. Oriti, and M. Colombini, "Optimized energy management system to reduce fuel consumption in remote military microgrids," *IEEE Trans. Ind. Appl.*, vol. 53, no. 6, pp. 5777–5785, Nov. 2017.
[13] J. G. Sprague, "Optimal scheduling of time-shiftable electric loads in expeditionary power grids," M.S. thesis, Naval Postgraduate School, Monterey, California, 2015.
[14] J. A. Olabode, "Analysis of the performance of an optimization model for time-shiftable electrical load scheduling under uncertainty," M.S. thesis, Naval Postgraduate School, Monterey, California, 2016.
[15] S. Shabshab, "Fuel-conserving environmental control strategies for small islanded microgrids," MIT S.M. thesis, Dept. Mech. Eng., Jun. 2018.
[16] C. Laughman *et al.*, "Power signature analysis," *IEEE Power Energy Mag.*, vol. 1, no. 2, pp. 56–63, Mar./Apr. 2003.
[17] M. Gillman *et al.*, "Accounting for every kilowatt," *Defense AT&L*, 2014.
[18] S. Shabshab, J. Nowocin, P. Lindahl, and S. Leeb, "Microgrid modeling and fuel savings opportunities through direct load control," in *Proc. 44th Annu. Conf. IEEE Ind. Electron. Soc.*, Oct. 2018, pp. 231–236.
[19] P. A. Lindahl, D. H. Green, G. Bredariol, A. Aboulian, J. S. Donnal, and S. B. Leeb, "Shipboard fault detection through nonintrusive load monitoring: A case study," *IEEE Sensors J.*, vol. 18, no. 21, pp. 8986–8995, Nov. 2018.
[20] D. Green *et al.*, "A multi-scale framework for nonintrusive load identification," *IEEE Trans. Ind. Informat.*, p. 1, 2019, doi:10.1109/TII.2019.2923236.
[21] S. C. Shabshab, P. A. Lindahl, J. K. Nowocin, and S. B. Leeb, "Voltage waveform transient identification for autonomous load coordination," *IEEE Access*, vol. 7, pp. 123–130, 2019.

Spencer C. Shabshab received the master's degree in mechanical engineering from the Massachusetts Institute of Technology, Cambridge, MA, USA, in 2018. He is currently a Submarine Officer in the United States Navy.

Peter A. Lindahl received the B.S. degree in electrical engineering from Penn State University, State College, PA, USA, in 2003, the M.S. degree in electrical engineering and the Ph.D. degree in engineering from Montana State University, Bozeman, MT, USA, in 2009 and 2013, respectively. He was with the Research Laboratory of Electronics, the Massachusetts Institute of Technology as a Postdoctoral Associate in 2014. He is currently a Senior Associate with the Electrical Engineering and Computer Science Practice, Exponent, Inc., where he provides technical consulting services regarding energy and power system operation, power system and machinery diagnostics and condition monitoring, and root-cause failure analysis and safety evaluation of industrial equipment, and consumer products.

Steven B. Leeb received the Ph.D. degree from the Massachusetts Institute of Technology, Cambridge, MA, USA, in 1993. Since 1993, he has been a member of the MIT faculty with the Department of Electrical Engineering and Computer Science. He also holds a joint appointment in MIT's Department of Mechanical Engineering. He is concerned with the development of signal processing algorithms for energy and real-time control applications.

J. Kendall Nowocin received the Ph.D. degree from the Massachusetts Institute of Technology, Cambridge, MA, USA, in 2017.